

ESS-ReduNet: Enhancing Subspace Separability of ReduNet via Dynamic Expansion with Bayesian Inference

Xiaojie Yu¹, Haibo Zhang¹, Lizhi Peng^{2,3}, Fengyang Sun⁴, Jeremiah Deng¹

¹University of Otago

²Quan Cheng Laboratory

³University of Jinan

⁴Victoria University of Wellington

yuxiaojie814@gmail.com, haibo.zhang@otago.ac.nz, plz@ujn.edu.cn, fengyang.sun@vuw.ac.nz, jeremiah.deng@otago.ac.nz

Abstract

ReduNet is a deep neural network model that leverages the principle of maximal coding rate **reduction** to transform original data samples into a low-dimensional, linear discriminative feature representation. Unlike traditional deep learning frameworks, ReduNet constructs its parameters explicitly layer by layer, with each layer’s parameters derived based on the features transformed from the preceding layer. Rather than directly using labels, ReduNet uses the similarity between each category’s spanned subspace and the data samples for feature updates at each layer. This may lead to features being updated in the wrong direction, impairing the correct construction of network parameters and reducing the network’s convergence speed. To address this issue, based on the geometric interpretation of the network parameters, this paper presents ESS-ReduNet to enhance the separability of each category’s subspace by dynamically controlling the expansion of the overall spanned space of the samples. Meanwhile, label knowledge is incorporated with Bayesian inference to encourage the decoupling of subspaces. Finally, stability, as assessed by the condition number, serves as an auxiliary criterion for halting training. Experiments on the ESR, HAR, Coverttype, and Gas datasets demonstrate that ESS-ReduNet achieves more than 10x improvement in convergence compared to ReduNet. Notably, on the ESR dataset, the features transformed by ESS-ReduNet achieve a 47% improvement in SVM classification accuracy.

1 Introduction

For a classification task, deep neural networks are designed to learn a nonlinear mapping through a sequence of layers, with the goal of accurately mapping data to their respective labels. A common practice in training deep learning models involves minimizing empirical risk by employing cross-entropy (CE) loss [Goodfellow *et al.*, 2016]. While CE loss is both effective and commonly used, fitting labels alone does not ensure

learning meaningful, structured representational information. In fact, recent studies [Papayan *et al.*, 2020; Fang *et al.*, 2021; Zhu *et al.*, 2021] show that the learned representations derived from the training using CE loss demonstrate a phenomenon of *neural collapse*: as the CE loss for every class gets close to zero, the representation of each class shrinks to a single point. The variability and structural details associated with each class are being stifled and ignored. Additionally, the development of deep network architectures often stems from extensive trial and error, lacking a solid basis in explicit mathematical principles.

To address the dual questions concerning the objectives of representation learning and the principles of network architecture design, Chan *et al.* [2022] introduced ReduNet, based on the lossy data coding and compression principles. They proposed that the objective function for representation learning should focus on extracting **low-dimensional, linear discriminative representation** from high-dimensional data. To learn linear discriminative representation, the following three principles are proposed: 1) intra-class compressible; 2) inter-class discriminative; 3) diverse representation where feature dimensions or variance within each class are maximized while remaining uncorrelated with features of other classes. The quality of this type of representation can be measured using a principled metric derived from the lossy data compression, termed **rate reduction**. The architecture of ReduNet is constructed layer by layer in a forward fashion, with the goal of maximizing the *rate reduction*. The parameters of each layer are constructed by the features transformed from the previous layer. Ideally, we expect the features of each class to update toward the subspaces spanned by the data of the corresponding class, with the subspaces becoming increasingly separated until they are mutually orthogonal.

Rather than directly using labels during training, ReduNet updates features based on estimated degree of membership by evaluating the similarities between the subspaces spanned by each class’s data and the samples. This helps to address the **inconsistency issue**: Unlike the backpropagation strategy, the forward manner optimization strategy of ReduNet dictates that if each layer during training directly uses labels for feature updates, testing samples cannot be updated due to the lack of labels. However, the estimated degree of membership can be highly inaccurate in the early layers of the network.

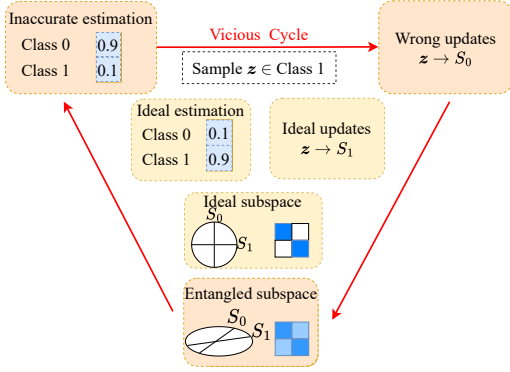


Figure 1: The Vicious Cycle of ReduNet. S_0 and S_1 are spanned subspaces of class 0 and class 1, respectively. $z \rightarrow S_0$ means sample z updating towards S_0 .

The inaccuracy of the estimation arises because the separability of subspaces may be compromised due to the limited overall spanned space. The constrained and entangled subspaces may fail to accurately estimate the degree of membership effectively. As illustrated in Figure 1, this leads to an incorrect update of features and inaccurate network parameters, further deteriorating the separability of the subspace and forming a vicious cycle. This also decreases the network’s convergence speed and the final classification accuracy of the transformed features. Besides, ReduNet needs to carefully manage early stopping for its training efficiency and quality. Firstly, if ReduNet is correctly constructed, the objective function stabilizes quickly, making additional layers unnecessary. Secondly, although the objective function of an incorrectly constructed ReduNet tends to be stable, the vicious cycle will continue to deteriorate the quality of features and the network. Therefore, relying solely on the objective function to stop training is unreasonable. In this paper, we present ESS-ReduNet, a framework that aims to enhance subspace separability to correct the feature updates and accelerate training with the following contributions:

1. To prioritize the expansion of the overall spanned space, we introduce a weight function to dynamically control the expansion process. This enhances the separability of subspaces across different classes in higher-dimensional space, thereby guiding the samples to update in the correct direction.
2. By comparing erroneous estimations with labels, the label knowledge is incorporated by Bayesian inference to correct the estimation of membership. Note that this introduces label knowledge while avoiding the inconsistency issue, as the posterior probabilities obtained through Bayesian inference during training retain the likelihood of errors in estimation functions, which can be reused during testing.
3. Given that ReduNet aims to flatten each category of data into its respective linear subspace, we use the condition number, an essential metric for testing whether a linear system is ill-conditioned, as an auxiliary criterion for stopping training. This helps save computational re-

sources and maintain feature quality.

4. Experiments on the HAR and ESR datasets demonstrate that our method accelerates the reduction of errors in estimating membership by a factor of 100 compared to ReduNet. Additionally, it speeds up network convergence by tenfold on the ESR, HAR, Covertype, and Gas datasets. Furthermore, on the ESR and Covertype datasets, the transformed features by our method achieved a 47% and 37% increase in SVM accuracy, respectively. Significant improvements were also observed in other datasets and with other classifiers (KNN, NSC).

2 Background

2.1 Overview of ReduNet

For the given finite data samples $\mathbf{X} = [\mathbf{x}^1, \dots, \mathbf{x}^m] \in \mathbb{R}^{D \times m}$, the compactness of the learned features $\mathbf{Z} = [\mathbf{z}^1, \dots, \mathbf{z}^m] \in \mathbb{R}^{n \times m}$ can be measured by the average coding length, i.e. the *coding rate* subject to the distortion ϵ :

$$R(\mathbf{Z}, \epsilon) \doteq \frac{1}{2} \log \det(\mathbf{I} + \frac{n}{m\epsilon^2} \mathbf{Z} \mathbf{Z}^T). \quad (1)$$

This measurement was proposed by Ma *et al.* [2007] based on the rate-distortion theory [Cover and Thomas, 2006]. Supposing \mathbf{Z} contains two **uncorrelated** subsets, \mathbf{Z}_1 and \mathbf{Z}_2 , the coding rate for all data $R(\mathbf{Z}_1 \cup \mathbf{Z}_2)$ is greater than the sum of the coding rates for $R(\mathbf{Z}_1)$ and $R(\mathbf{Z}_2)$. Furthermore, if \mathbf{Z}_1 is **orthogonal** to \mathbf{Z}_2 , the difference $R(\mathbf{Z}_1 \cup \mathbf{Z}_2) - (R(\mathbf{Z}_1) + R(\mathbf{Z}_2))$ is approximately maximized.

For a classification problem involving k classes, Chan *et al.* [2022] proposed ReduNet, which aims to perform classification by implementing a series of transformations that orthogonalize the samples across different classes. Hence, *maximal coding rate reduction* (MCR²) is proposed as the objective function:

$$\Delta R(\mathbf{Z}, \mathbf{\Pi}, \epsilon) = R(\mathbf{Z}, \epsilon) - R_c(\mathbf{Z}, \epsilon | \mathbf{\Pi}) \quad (2)$$

$R(\mathbf{Z}, \epsilon) = \frac{1}{2} \log \det(\mathbf{I} + \alpha \mathbf{Z} \mathbf{Z}^T)$ aims to maximize the spanned space volume (or dimension) of the whole set \mathbf{Z} such that features of different classes are incoherent to each other (i.e. inter-class discriminative). $-R_c(\mathbf{Z}, \epsilon | \mathbf{\Pi}) = -\sum_{j=1}^k \frac{\gamma_j}{2} \log \det(\mathbf{I} + \alpha_j \mathbf{Z} \mathbf{\Pi}^j \mathbf{Z}^T)$ aims to minimize the spanned space volume of each class such that features within the same class are highly correlated (i.e. intra-class compressible). Here, $\mathbf{\Pi} = \{\mathbf{\Pi}^j \in \mathbb{R}^{m \times m}\}_{j=1}^k$ is defined as a group of diagonal matrices, which are used to encode the membership of m samples within k different classes. Specifically, $\mathbf{\Pi}^j(i, i)$ represents the probability of the i^{th} sample belonging to j^{th} subset. Similar to the denotation in [Chan *et al.*, 2022], $\alpha = \frac{n}{m\epsilon^2}$, $\alpha_j = \frac{n}{\text{tr}(\mathbf{\Pi}^j)\epsilon^2} \gamma_j = \frac{\text{tr}(\mathbf{\Pi}^j)}{m}$ for $j = 1, \dots, k$.

To maximize MCR², a gradient ascent method based on the derivatives of the objective function Eq. (2) is used for feature updates:

$$\frac{\partial \Delta R}{\partial \mathbf{Z}} \Big|_{\mathbf{z}_\ell} = \underbrace{\mathbf{E}_\ell}_{\text{Expansion}} \mathbf{z}_\ell - \sum_{j=1}^k \gamma_j \underbrace{\mathbf{C}_\ell^j}_{\text{Compression}} \mathbf{z}_\ell \mathbf{\Pi}^j. \quad (3)$$

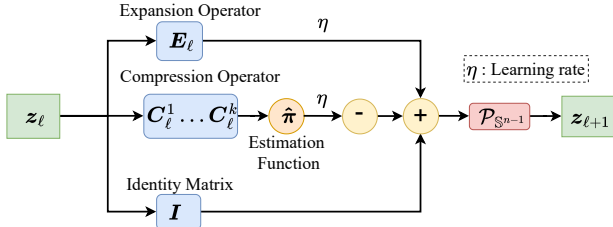


Figure 2: A Layer of ReduNet

Here, $\mathbf{E}_\ell = \alpha(\mathbf{I} + \alpha \mathbf{Z}_\ell \mathbf{Z}_\ell^T)^{-1} \in \mathbb{R}^{n \times n}$ and $\mathbf{C}_\ell^j = \alpha_j(\mathbf{I} + \alpha_j \mathbf{Z}_\ell \mathbf{\Pi}^j \mathbf{Z}_\ell^T)^{-1} \in \mathbb{R}^{n \times n}$. Thereby, for a feature \mathbf{z}_ℓ , the increment transform $g(\cdot, \boldsymbol{\theta}_\ell)$ on the ℓ -th layer is defined as:

$$\mathbf{z}_{\ell+1} \propto \mathbf{z}_\ell + \eta \cdot g(\mathbf{z}_\ell, \boldsymbol{\theta}_\ell) \quad \text{subject to} \quad \mathbf{z}_{\ell+1} \in \mathbb{S}^{n-1}. \quad (4)$$

$$g(\mathbf{z}_\ell, \boldsymbol{\theta}_\ell) = \mathbf{E}_\ell \mathbf{z}_\ell - \sum_{j=1}^k \gamma_j \mathbf{C}_\ell^j \mathbf{z}_\ell \hat{\pi}^j(\mathbf{z}_\ell) \in \mathbb{R}^n. \quad (5)$$

Note that unlike Eq.3, Eq.5 uses estimation functions $\{\hat{\pi}^j\}_{j=1}^k$ for feature updates instead of directly using the labels. This allows us to consistently use the same estimation functions for feature updates during the testing, without worrying about the inconsistency issues that may arise from directly using the labels. Hence, as shown in Figure 2, ReduNet is built in a layer-by-layer forward manner. For the ℓ -th layer, the parameters (i.e., expansion operators \mathbf{E}_ℓ and compression operators $\{\mathbf{C}_\ell^j\}_{j=1}^k$) are constructed by transformed features \mathbf{Z}_ℓ of previous layer. All features are then updated by \mathbf{E}_ℓ and $\{\mathbf{C}_\ell^j\}_{j=1}^k$. Ultimately, the objective is to ensure that the transformed features from different classes are orthogonal to each other.

In practice, under the assumption that signals are sparsely generated, ReduNet introduces a *lifting* operation, which involves convolving the samples with N_c filters to obtain features across N_c channels. This *lifting* operation expands the upper limit of the spanned space's dimensions, transforming from the original $\mathbb{R}^{n \times m}$ to $\mathbb{R}^{N_c \times n \times m}$. Nevertheless, for some challenging datasets, ReduNet fails to fully utilize the expanded space because the rank of the spanned space does not increase sufficiently (at most $N_c \times n \times m$), and as a result, it continues to transform features within a constrained, smaller space. This hinders the sufficient expansion of the subspaces for each class (i.e., the separation between subspaces), thereby affecting the accurate estimation of the degree of membership and leading to incorrect feature updates.

2.2 Related Works

Efforts on Subspace Representation Learning

A common belief is that the data from each class exhibit a low-dimensional intrinsic structure, and the role of deep networks is to learn these structures [Hinton and Salakhutdinov, 2006]. Although many efforts seek to directly impose subspace structures on features learned by deep networks [Ji *et al.*, 2017; Peng *et al.*, 2017; Lezama *et al.*, 2018; Zhou *et al.*, 2018; Zhang *et al.*, 2019a; Zhang *et al.*, 2019b], the subspace properties explored in these studies do not fulfill the three principles mentioned in section 1 [Haeffele *et al.*,

2021]. In contrast, the representation derived from the optimized MCR² objective function exhibits the desired characteristics.

Attempts on Architecture Explanation

Chan *et al.* [2022] also aim to explain components of deep networks within a unified theoretical framework, such as convolutions [LeCun *et al.*, 1998; Krizhevsky *et al.*, 2012], skip connection [He *et al.*, 2016], nonlinear activation functions, etc. They established a connection between deep convolutional networks and invariant rate reduction. Using the relationship between the circulant matrix and the convolution operation, the deep network derived from MCR² could naturally transition to a deep convolutional network. *Sparse rate reduction* can also be used to construct white-box transformers, which bridge compression, denoising, and multi-head self-attention [Yu *et al.*, 2023b; Yu *et al.*, 2023a]. In addition, the relationship between the circulant matrix and the discrete Fourier transform can be utilized to develop a **Fourier version** of ReduNet. Due to the slower convergence speed of the Fourier version of ReduNet, this paper primarily focuses on the basic version of ReduNet. However, our **plug-in** approach is equally applicable to the Fourier version, as our improvements solely involve adjusting the weights of the expansion operators and correcting errors in estimating labels.

ReduNet suffers from the limitations of a low-volume spanned space and errors in estimating membership. We will discuss these issues in detail in the next section. Furthermore, we will show that relying solely on incorporating label knowledge to correct network training quickly leads to stagnation. Further expansion of the spanned space is necessary to correct and accelerate network training. This work highlights the relative importance of expansion operations: *only a sufficiently large overall data span can support the compression and transformation of individual subspaces; otherwise, in particularly small spaces, subspaces can easily become entangled.*

3 Motivation

To demonstrate the motivation, the Kaggle version [2018] of the ESR [Qiuyi Wu, 2017] dataset serves as a case study of the binary classification problem, distinguishing between instances with and without epileptic seizures. After balancing by random undersampling, each class containing 1,456 samples, with each sample having 178 dimensions.

Motivation 1: *constrained and entangled subspaces reduce the accuracy of estimation functions, thereby hindering the correct updating of features and the proper construction of the network parameters.* As shown in Eq.5, to ensure consistency between the training and testing, ReduNet uses k estimation functions $\{\hat{\pi}^j\}_{j=1}^k$ to approximate membership functions $\{\pi^j\}_{j=1}^k$, where

$$\hat{\pi}^j(\mathbf{z}_\ell^i) \doteq \frac{\exp(-\lambda \|\mathbf{C}_\ell^j \mathbf{z}_\ell^i\|)}{\sum_{j=1}^k \exp(-\lambda \|\mathbf{C}_\ell^j \mathbf{z}_\ell^i\|)} \in [0, 1]; \quad (6)$$

Essentially, these functions estimate membership of samples based on the similarity between the subspaces of the k classes

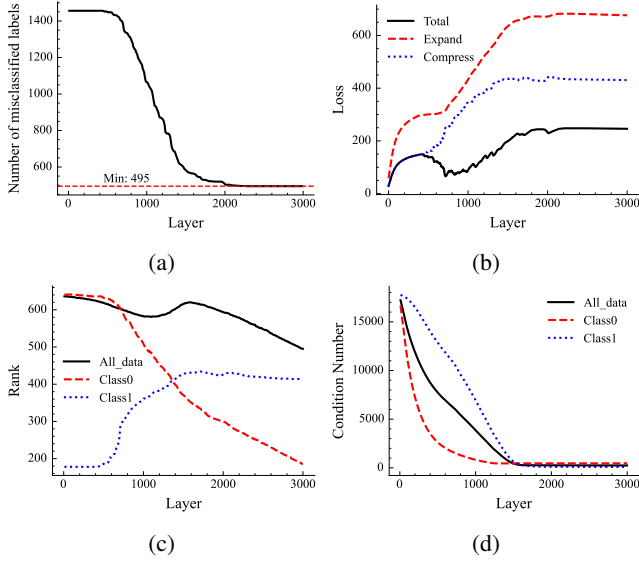


Figure 3: (a): The number of misclassified labels of $\{\hat{\pi}^j\}_{j=1}^k$; (b): Objective function curve; (c): Rank trend; (d): Condition number trend.

and the samples. As the Figure 3a shows, although the misclassification rate of estimation functions decreases with more layers, these functions still can not provide correct estimations for some challenging samples. Besides, Figure 3b shows the curve of objective function MCR^2 . The *Expand* curve corresponds to $R(\mathbf{Z}, \epsilon)$ of Eq. (2), while the *Compress* curve corresponds to $R_c(\mathbf{Z}, \epsilon | \mathbf{\Pi})$ of Eq. (2). The *Total* curve represents the value of the MCR^2 function. It can be observed that the *Total* curve overlaps with the *Compress* curve approximately before the 500th layer. We identified this as an extreme case of the estimation function’s failure, referred to as the *lopsided* issue. This occurs when samples from one class (Class 1) are incorrectly classified by the estimation function into another class (Class 0), resulting in erroneous updates for all samples of the misclassified class. Specifically, samples from Class 1 are only compressed by the compression operator C_ℓ^0 . Furthermore, the network parameters constructed by the degraded feature are inappropriate.

Motivation 2: *suboptimal estimation functions decrease the network’s convergence speed, and the objective function should not be the sole criterion for assessing network convergence.* Figures 3a and 3b demonstrate that ReduNet requires more than 2000 layers to achieve convergence. Nevertheless, the ranks of the data matrices continues to decline after 2000 layers, as illustrated in Figure 3c. This indicates that further training of a poorly constructed network degrades feature quality. Inspired by [Curth *et al.*, 2023], the condition numbers of the matrices $(\mathbf{I} + \alpha \mathbf{Z}_\ell \mathbf{Z}_\ell^*)$ and $\{(\mathbf{I} + \alpha_j \mathbf{Z}_\ell \mathbf{\Pi}^j \mathbf{Z}_\ell^*)\}_{j=1}^k$ in the \mathbf{E}_ℓ and $\{C_\ell^j\}_{j=1}^k$ are measured, as depicted in Figure 3d. The condition number stabilizes around the 1600th layer, earlier than the objective function at 2000 layers. Hence, the changes of condition number can be an auxiliary criterion to halt training. This helps save

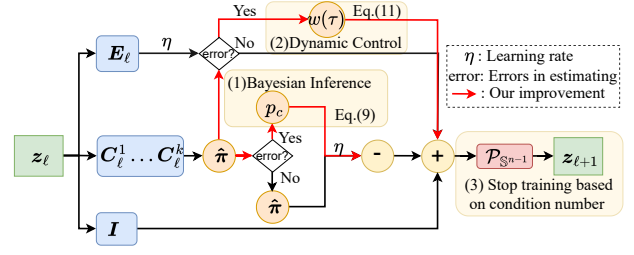


Figure 4: Overview of ESS-ReduNet

computational resources and maintain feature quality.

4 ESS-ReduNet

Three questions need to be addressed:

1. Can we introduce labels to guide feature updates in a relatively correct direction without causing the inconsistency issue?
2. Besides using labels, are there other methods to improve the accuracy of estimation functions?
3. Are there other metrics that can be used to assist in determining when to stop training?

4.1 Incorporate Label Knowledge

A straightforward approach to addressing the inaccuracy of the estimation function is to use labels for correcting the estimates. However, this can easily introduce inconsistency issues once again. What we aim for is to find a method that can both use label knowledge to guide feature updates and allow for the reuse of this information during the test phase. By combining the labels with the estimates of the estimation function, we can calculate the average performance of the estimation function on samples from each class, and infer the posterior probability based on the labels: when a sample is observed to be classified into class i , what is the probability that it actually belongs to class j ? We can treat this posterior probability as containing certain label knowledge, which can be directly reused during the test phase. Hence, Bayesian inference is employed to incorporate the label knowledge.

The underlying intuition is to first count the samples misclassified by estimation functions, and then by comparing with the labels, infer the posterior probability that a sample observed to be classified into class C_j (i.e. $z_\ell \rightarrow C_j$) actually belongs to class C_i (i.e. $z_\ell \in C_i$): $p^{ij} = P(z_\ell \in C_i | z_\ell \rightarrow C_j)$.

$$p^{ij} = \frac{P(z_\ell \in C_i)P(z_\ell \rightarrow C_j | z_\ell \in C_i)}{\sum_i P(z_\ell \rightarrow C_j | z_\ell \in C_i)P(z_\ell \in C_i)} \quad (7)$$

Given that this study uses balanced datasets with k classes, the prior probability $P(z_\ell \in C_i) = \frac{1}{k}$. For samples of class i , the probability of being classified into class j , i.e. $P(z_\ell \rightarrow C_j | z_\ell \in C_i)$ in Eq.7, is defined as the average probability of all samples in class i being assigned by the estimation function $\hat{\pi}^j$ during the training process:

$$P(z_\ell \rightarrow C_j | z_\ell \in C_i) = \frac{1}{m_i} \sum_{l=1}^{m_i} \hat{\pi}^j(z_\ell^l) \quad (8)$$

Here, m_i is the number of samples in class i . Therefore, for a sample z_ℓ , we use the corrected estimation $p_c^i(z_\ell) = P_c(z_\ell \in C_i)$ as the weight for the compression operator C_ℓ^i :

$$p_c^i(z_\ell) = \sum_{j=1}^k P(z_\ell \in C_i | z_\ell \rightarrow C_j) P(z_\ell \rightarrow C_j) \quad (9)$$

Here, $P(z_\ell \rightarrow C_j) = \hat{\pi}^j(z_\ell)$ represents the estimated probability that the sample z_ℓ belongs to class j , as derived from the estimation function.

Although Bayesian inference can correct the estimation ideally, the overall spanned space may not expand promptly, preventing further decoupling of the subspaces and leading to stagnation of the training process. Figure 9a from the ablation study confirms this assumption. Consequently, dynamic control of the expansion is introduced next.

4.2 Control the Expansion Dynamically

Analysis of the Geometric Interpretation of Expansion Operators

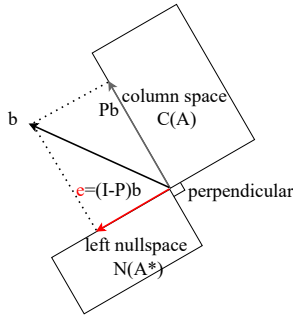


Figure 5: The Geometric Interpretation of Least Squares

$E_\ell z_\ell$ can be considered as approximately equivalent to the residual of z_ℓ projected onto the complement of the spanned space. $z_\ell = z_\ell + \eta E_\ell z_\ell$ represents the sample moving towards the complement of the span, thereby increasing the ranks of Z_ℓ and $\{Z_\ell \Pi^j\}_{j=1}^k$, expanding the spanned space. In contrast, $z_\ell = z_\ell - \eta C_\ell^j z_\ell$ shifts the sample towards the span of class j , compressing the spanned subspace. This can be verified by the equation below:

$$\begin{aligned} E_\ell z_\ell &= \alpha(z_\ell - Z_\ell [\beta_\ell]_*) \\ &= \alpha(I - \alpha Z_\ell (I + \alpha Z_\ell^T Z_\ell)^{-1} Z_\ell^T) z_\ell \end{aligned} \quad (10)$$

where $[\beta_\ell]_* = \alpha(I + \alpha Z_\ell^T Z_\ell)^{-1} Z_\ell^T z_\ell$. Eq.10 is exactly the *residuals* of the ridge regression problem $[\beta_\ell]_* = \arg \min_{\beta_\ell} \alpha \|z_\ell - Z_\ell \beta_\ell\|_2^2 + \|\beta_\ell\|_2^2$. Since the loss function of ridge regression is essentially a least squares function with an L2 norm regularization term, we can explain the geometric meaning of $E_\ell z_\ell$ by comparing it to the geometric interpretation of least squares. As shown in Figure 5, for a classical least squares problem of $Ax = b$, the projection matrix $I - P = I - A(A^T A)^{-1} A^T$ projects vector b onto the complement of column space $C(A)$, namely the left nullspace $N(A^T)$, and the projection is the error (or residual) $e = (I - P)b$ [Strang, 2012]. Thus, this confirms the

geometric interpretation of $E_\ell z_\ell$. For a detailed derivation, please see Appendix A.

As mentioned in the Background section, while the *lifting* operation increases the upper limit of the dimensions of the spanned space, it is the expansion operator that truly enlarges the spanned space. Adequate expansion of the space is crucial to ensure the decoupling of various class subspaces and to ensure that samples are compressed into the correct subspaces. This highlights the greater importance of the expansion operator compared to the compression operator. Therefore, we introduce a weight function to dynamically control the expansion process.

Weight Function for Controlling Expansion Dynamically

A straightforward strategy is to enlarge the expansion when training faces stagnation. However, this still results in samples undergoing incorrect transformations across multiple layers. Therefore, it is preferable to minimize the misclassification rate of the estimation functions as quickly as possible. When errors in membership estimation are present, we tentatively expand the space slowly. This helps maintain the compactness of samples within classes and facilitates effective ongoing training. However, we also seek to rapidly reduce the misclassification rate of the estimated function to prevent excessive updates in the wrong direction. Thus, we introduce a truncated, monotonically increasing exponential function as the weight function $w(\tau_\ell)$ of the expansion operator E_ℓ , where

$$w(\tau_\ell) = \min(\exp(\tau_\ell), u) \in [1, u], \tau_\ell \in [0, \infty). \quad (11)$$

Here, τ_ℓ increases with the number of layers, indicating that if the subspaces do not decouple promptly, the weight of the expansion operator should be increased to facilitate more extensive expansion. The product of u and the learning rate η should be less than or equal to 1 to avoid excessively large gradients. Specifically, when $\eta = 0.1$, u can be set to 10.

It is important to emphasize that the gradient update $g(z_\ell, \theta_\ell)$ of features is jointly determined by $E_\ell z_\ell$ and $-\sum_{j=1}^k \gamma_j C_\ell^j z_\ell \pi^j(z_\ell)$. Due to their sum potentially being small or even zero, this can result in small or vanishing gradients. Therefore, increasing the weight of the expansion operator E_ℓ helps enhance the magnitude of the gradient $g(z_\ell, \theta_\ell)$ and expand the overall spanned space, improving the separability of subspaces and the accuracy of the estimation function.

4.3 Condition Number for Stopping training

In addition to the objective function, the stability of network parameters can serve as a criterion for assessing network convergence. A lower condition number indicates a more stable linear system and can serve as an auxiliary criterion to halt training.

For a ridge regression problem $[\beta]_* = \arg \min_{\beta} (\|y - X\beta\|_2^2 + \lambda \|\beta\|_2^2)$, the condition number is given by $\kappa(X^T X + \lambda I) = \frac{\sigma_{\max}}{\sigma_{\min}}$. Here, σ_{\max} and σ_{\min} are the maximum and minimum singular values of $X^T X + \lambda I$, respectively [Tabert *et al.*, 2019]. Due to the previously analyzed connection between ridge regression and network

parameters, $k + 1$ condition numbers of $(\mathbf{I} + \alpha \mathbf{Z}_\ell \mathbf{Z}_\ell^T)$ and $\{(\mathbf{I} + \alpha_j \mathbf{Z}_\ell \mathbf{\Pi}^j \mathbf{Z}_\ell^T)\}_{j=1}^k$ in the \mathbf{E}_ℓ and $\{\mathbf{C}_\ell^j\}_{j=1}^k$ are measured to track the stability of the network. The condition number decreases as the number of layers increases. When there is no significant change in the condition numbers, it is considered that the network has converged, and training can be stopped. In practice, since calculating condition numbers is computationally intensive, it is feasible to assess the stability of network parameters every several tens of layers.

4.4 Algorithm Pseudocode

Algorithm 1 Training Phase

Input: $X = [x^1, \dots, x^m] \in \mathbb{R}^{D \times m}$, $\mathbf{\Pi}$, $\epsilon > 0$, λ , η .

Output: \mathbf{Z}_{L+1} , $\{\mathbf{E}_\ell\}_{\ell=1}^L$, $\{\mathbf{C}_\ell^j\}_{j=1, \ell=1}^{k, L}$, $\{w_\ell\}_{\ell=1}^L$,

$\{p_\ell^{ij}\}_{i=1, j=1, \ell=1}^{k, k, L}$.

```

1: Set  $\mathbf{Z}_1 = [\mathbf{z}_1^1, \dots, \mathbf{z}_1^m] = \mathbf{X} \in \mathbb{R}^{n \times m}$ ,  $\tau = 0$ .
2: for  $\ell = 1, \dots, L$  do
3:   Compute parameters  $\mathbf{E}_\ell$  and  $\{\mathbf{C}_\ell^j\}_{j=1}^k$ .
4:   Assess the error rates of the estimation functions.
5:   if have errors then
6:     Compute posterior probability  $\{p_\ell^{ij}\}_{i=1, j=1}^{k, k}$ 
7:     for  $i = 1, \dots, m$  do
8:       Compute corrected estimations  $\{p_c^j(\mathbf{z}_\ell^i)\}_{j=1}^k$ .
9:       # Controlling expansion dynamically
10:       $w_\ell(\tau_\ell) = \min(\exp(\tau_\ell), u)$ 
11:       $\mathbf{z}_{\ell+1}^i = \mathcal{P}_{S^{n-1}}(\mathbf{z}_\ell^i + \eta(w_\ell \mathbf{E}_\ell \mathbf{z}_\ell^i - \sum_{j=1}^k \gamma_j \mathbf{C}_\ell^j \mathbf{z}_\ell^i p_c^j(\mathbf{z}_\ell^i)))$ ;
12:     end for
13:      $\tau_{\ell+1} = \tau_\ell + 0.1$ 
14:   else if do not have errors then
15:     for  $i = 1, \dots, m$  do
16:        $\mathbf{z}_{\ell+1}^i = \mathcal{P}_{S^{n-1}}(\mathbf{z}_\ell^i + \eta(\mathbf{E}_\ell \mathbf{z}_\ell^i - \sum_{j=1}^k \gamma_j \mathbf{C}_\ell^j \mathbf{z}_\ell^i \bar{\pi}^j(\mathbf{z}_\ell^i)))$ ;
17:     end for
18:   end if
19:   if no change on condition number then
20:     stop training
21:   end if
22: end for

```

As the Algorithm 1 shows, the errors of the estimation functions are calculated (line 4). If there are misclassified samples, incorporation of label knowledge and the dynamic control of expansion are employed (lines 5-13). Otherwise, the original method is executed (lines 14-18). Condition number serves as an auxiliary criterion for stopping training (lines 19-21) and does not need to be computed at every layer. Moreover, Bayesian inference and dynamic expansion only involve basic arithmetic operations. Therefore, ESS-ReduNet does not significantly increase the computational load. The detailed condition number curves presented in the experimental section are intended solely to highlight the acceleration effects of ESS-ReduNet.

5 Experiments

ESS-ReduNet is evaluated on seven datasets: HAR [Jorge Reyes-Ortiz, 2012], ESR [Qiuyi Wu, 2017], Covtype (C)

[Blackard, 1998], Gas [Vergara, 2012], mfeatFactors and mfeatFourier [Duin, 1998], musk [David Chapman, 1994]. We use $\epsilon^2 = 0.1$ and $\eta = 0.1$ for all datasets. The initial number of layers is set to 3000, which is sufficient to highlight the strengths of our method.

A case study on the ESR dataset is used to demonstrate how our method accelerates network training and produces higher-quality features. In addition, an ablation study is conducted to underscore the necessity of Bayesian inference and dynamic control of the expansion. Finally, based on [Yu *et al.*, 2020], we detail the classification accuracy of Support Vector Machine (SVM), K-Nearest Neighbors (KNN), and Nearest Subspace Classifier (NSC) across seven datasets, demonstrating the acceleration and corrective benefits of ESS-ReduNet.

5.1 Case Study

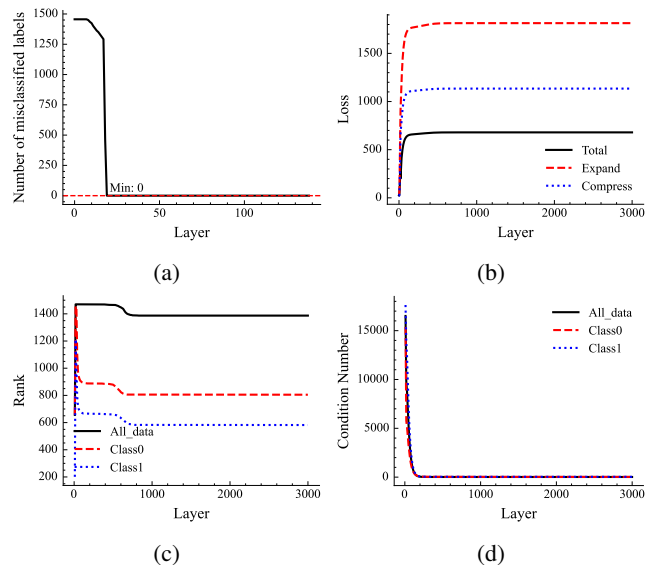


Figure 6: Performance of ESS-ReduNet on ESR Dataset.

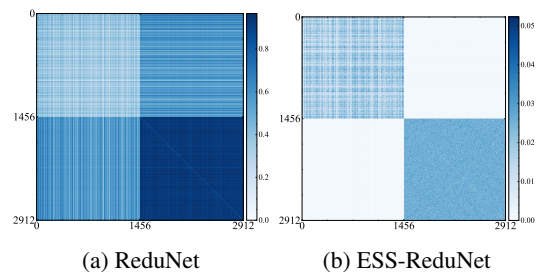


Figure 7: Visualization of ESR Feature Orthogonalization at the 200th Layer. Heatmap of $|\mathbf{Z}\mathbf{Z}^*|$ showing correlation levels: darker shades indicate higher correlation between two samples. Ideally, the subspaces of two classes should be orthogonal, evident as a block diagonal structure.

Same with the Figure 3, four aspects are evaluated on ESS-ReduNet. Notably, the number of misclassified samples rapidly decreases, reaching zero by the 19th layer as shown

in Figure 6a. In comparison, ReduNet required 2000 layers to reduce the misclassification count to 495, as demonstrated in Figure 3a, highlighting the accelerated network convergence achieved with ESS-ReduNet. Besides, as illustrated in Figure 6b, our method also achieves a higher MCR^2 value.

Figure 6c confirms that ESS-ReduNet effectively increases the rank of the linear space and expands the spanned space. The dimensions of the spanned spaces for the two classes add up to the total space dimension. As evident in Figure 7b, the two subspaces are now complementary and occupy the entire space. This suggests that, according to Figure 6d, it is reasonable to halt network training when there is no significant change in the condition number, which occurs around the 200th layer.

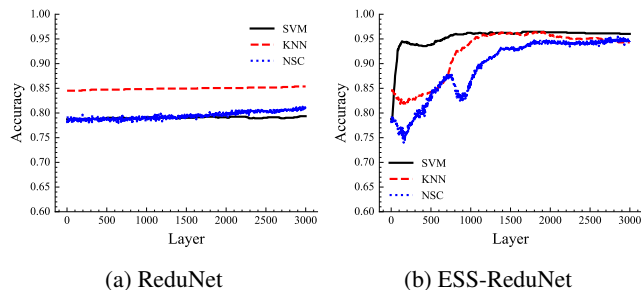


Figure 8: Performance Comparison on the Fourier Version.

In fact, our improvements is a plug-in approach that can be conveniently combined with the Fourier version of ReduNet. Although the convergence rate of the Fourier version is significantly slower, we have tested our method on the Fourier version as well. By comparing Figures 8a and 8b, it is evident that our method achieves higher accuracy.

5.2 Ablation Study

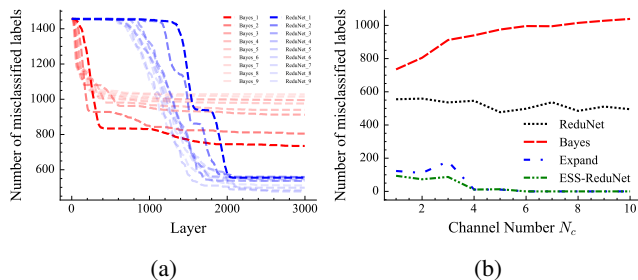


Figure 9: (a):The misclassification number of estimation functions for both the *Bayes* method (red line) and ReduNet (blue line). Different opacities represent varying channel numbers N_c of *lifting* operation; As N_c increases, the color becomes lighter. (b):The lowest number of misclassified samples by estimation functions for four methods, under different channel numbers N_c .

The following combinatorial approaches are evaluated to show the necessity of the Bayesian inference and dynamic expansion modules: ReduNet with Bayesian inference (*Bayes*), ReduNet with expansion dynamically (*Expand*), ESS-ReduNet and ReduNet. As shown by the red

line in Figure 9a, the *Bayes* method accelerates the reduction of misclassified samples compared to ReduNet, but subsequently reaches a plateau, exhibiting a phenomenon similar to gradient vanishing. Nevertheless, as displayed in Figure 9b, the ESS-ReduNet performs better under conditions of lower channel numbers than *Expand* method. This indicates that enlarged spanned space at higher channel numbers enhances subspaces' separability. In contrast, under low channel conditions, the label knowledge from *Bayes* method demonstrates its effectiveness in a limited spanned space.

Furthermore, Figure 9a shows that as the channel number increases, both the *Bayes* method and the ReduNet demonstrate a faster decline in the estimation function's error, as evidenced by the leftward shift of the red and blue curves. This observation confirms our theoretical analysis, suggesting that a higher number of channels, indicative of more convolutional kernels, provides additional bases that enhance the separation of samples across different classes.

5.3 Performance on Classification Tasks

Dataset	MCR^2	SVM	KNN	NSC	Layer
ESR	245.89	0.65	0.63	0.72	> 3000
	660.84	0.96	0.78	0.78	199
HAR	989.27	0.68	0.75	0.73	> 3000
	1066.02	0.70	0.75	0.75	326
Coverttype	108.09	0.54	0.71	0.56	> 3000
	295.79	0.74	0.74	0.71	219
Gas	147.12	0.98	0.99	0.95	> 3000
	889.90	0.97	0.97	0.96	94
mfeatFactors	603.38	0.97	0.97	0.97	194
	1011.57	0.97	0.97	0.97	125
mfeatFourier	668.10	0.82	0.82	0.82	134
	727.35	0.82	0.82	0.82	134
musk	481.99	0.93	0.93	0.93	164
	624.44	0.91	0.93	0.93	119

Table 1: Comparative results on MCR^2 , accuracy on three classifiers (higher value is better) and the layer of stopping training (lower value is better), with the first row showing outcomes from ReduNet and the second row presenting results of ESS-ReduNet.

Table 1 displays the test results of ESS-ReduNet across seven datasets. The *Layer* column indicates the convergence in the condition number. As shown in the table, ESS-ReduNet achieves higher MCR^2 values across all datasets. Besides, it allows training to stop earlier than ReduNet. Finally, ESS-ReduNet has achieved varying degrees of improvement in accuracy on three basic classifiers, or achieves acceleration while maintaining comparable accuracy to ReduNet.

6 Conclusion

This paper addresses issues arising from inaccurate estimation functions in ReduNet, such as incorrect feature updates, slow training, and the resultant poor quality of network structures and transformed features. The performance of the estimation functions depends on the separability of the subspaces of various classes. Hence, we propose the ESS-ReduNet: a

improved framework aims to enhance the subspace separability via controlling the expansion dynamically and incorporating the label knowledge through Bayesian inference. Both encourage the decoupling of subspaces, thereby improving the estimation performance. Finally, we track changes in the condition number of network parameters as a criterion to halt network training. As a plug-in approach, our improvements can be easily integrated with the Fourier version of ReduNet. Experimental results show that our method significantly accelerates network training, improves feature quality, and conserves computational resources.

References

- [Blackard, 1998] Jock Blackard. Covertypes, 1998.
- [Chan *et al.*, 2022] Kwan Ho Ryan Chan, Yaodong Yu, Chong You, Haozhi Qi, John Wright, and Yi Ma. ReduNet: A white-box deep network from the principle of maximizing rate reduction. *The Journal of Machine Learning Research*, 23(1):4907–5009, 2022. Publisher: JMLR.ORG.
- [Cover and Thomas, 2006] Thomas M. Cover and Joy A. Thomas. *Elements of Information Theory*. Wiley, July 2006.
- [Curth *et al.*, 2023] Alicia Curth, Alan Jeffares, and Mihaela van der Schaar. A U-turn on Double Descent: Rethinking Parameter Counting in Statistical Learning, October 2023. arXiv:2310.18988 [cs, stat].
- [David Chapman, 1994] Ajay Jain David Chapman. Musk (Version 2), 1994.
- [Duin, 1998] Robert Duin. Multiple Features, 1998.
- [Fang *et al.*, 2021] Cong Fang, Hangfeng He, Qi Long, and Weijie J. Su. Exploring deep neural networks via layer-peeled model: Minority collapse in imbalanced training. *Proceedings of the National Academy of Sciences*, 118(43):e2103091118, October 2021. Publisher: Proceedings of the National Academy of Sciences.
- [Goodfellow *et al.*, 2016] Ian Goodfellow, Yoshua Bengio, and Aaron Courville. *Deep learning*. MIT press, 2016.
- [Haeffele *et al.*, 2021] Benjamin D. Haeffele, Chong You, and René Vidal. A Critique of Self-Expressive Deep Subspace Clustering, March 2021. arXiv:2010.03697 [cs].
- [He *et al.*, 2016] Kaiming He, Xiangyu Zhang, Shaoqing Ren, and Jian Sun. Deep residual learning for image recognition. In *Proceedings of the IEEE conference on computer vision and pattern recognition*, pages 770–778, 2016.
- [Hinton and Salakhutdinov, 2006] G. E. Hinton and R. R. Salakhutdinov. Reducing the Dimensionality of Data with Neural Networks. *Science*, 313(5786):504–507, July 2006.
- [Ji *et al.*, 2017] Pan Ji, Tong Zhang, Hongdong Li, Mathieu Salzmann, and Ian Reid. Deep subspace clustering networks. *Advances in neural information processing systems*, 30, 2017.
- [Jorge Reyes-Ortiz, 2012] Davide Anguita Jorge Reyes-Ortiz. Human Activity Recognition Using Smartphones, 2012.
- [Krizhevsky *et al.*, 2012] Alex Krizhevsky, Ilya Sutskever, and Geoffrey E. Hinton. Imagenet classification with deep convolutional neural networks. *Advances in neural information processing systems*, 25, 2012.
- [LeCun *et al.*, 1998] Yann LeCun, Léon Bottou, Yoshua Bengio, and Patrick Haffner. Gradient-based learning applied to document recognition. *Proceedings of the IEEE*, 86(11):2278–2324, 1998. Publisher: Ieee.
- [Lezama *et al.*, 2018] José Lezama, Qiang Qiu, Pablo Musé, and Guillermo Sapiro. Ole: Orthogonal low-rank embedding—a plug and play geometric loss for deep learning. In *Proceedings of the IEEE Conference on Computer Vision and Pattern Recognition*, pages 8109–8118, 2018.
- [Ma *et al.*, 2007] Yi Ma, Harm Derksen, Wei Hong, and John Wright. Segmentation of Multivariate Mixed Data via Lossy Data Coding and Compression. *IEEE Transactions on Pattern Analysis and Machine Intelligence*, 29(9):1546–1562, September 2007.
- [Papayan *et al.*, 2020] Vardan Papayan, X. Y. Han, and David L. Donoho. Prevalence of neural collapse during the terminal phase of deep learning training. *Proceedings of the National Academy of Sciences*, 117(40):24652–24663, October 2020.
- [Peng *et al.*, 2017] Xi Peng, Jiashi Feng, Shijie Xiao, Jiwen Lu, Zhang Yi, and Shuicheng Yan. Deep Sparse Subspace Clustering, September 2017. arXiv:1709.08374 [cs].
- [Qiuyi Wu, 2017] Ernest Fokoue Qiuyi Wu. Epileptic Seizure Recognition, 2017.
- [Strang, 2012] Gilbert Strang. *Linear algebra and its applications*. 2012.
- [Tabeart *et al.*, 2019] Jemima M. Tabert, Sarah L. Dance, Amos S. Lawless, Nancy K. Nichols, and Joanne A. Waller. Improving the condition number of estimated covariance matrices, October 2019. arXiv:1810.10984 [math, stat].
- [Ur-Rashid, 2018] Harun Ur-Rashid. Epileptic Seizure Recognition, 2018.
- [van Wieringen, 2023] Wessel N. van Wieringen. Lecture notes on ridge regression, June 2023. arXiv:1509.09169 [stat].
- [Vergara, 2012] Alexander Vergara. Gas Sensor Array Drift at Different Concentrations, 2012.
- [Yu *et al.*, 2020] Yaodong Yu, Kwan Ho Ryan Chan, Chong You, Chaobing Song, and Yi Ma. Learning Diverse and Discriminative Representations via the Principle of Maximal Coding Rate Reduction. In H. Larochelle, M. Ranzato, R. Hadsell, M. F. Balcan, and H. Lin, editors, *Advances in Neural Information Processing Systems*, volume 33, pages 9422–9434. Curran Associates, Inc., 2020.
- [Yu *et al.*, 2023a] Yaodong Yu, Sam Buchanan, Druv Pai, Tianzhe Chu, Ziyang Wu, Shengbang Tong, Hao Bai,

Yuexiang Zhai, Benjamin D. Haeffele, and Yi Ma. White-Box Transformers via Sparse Rate Reduction: Compression Is All There Is?, November 2023. arXiv:2311.13110 [cs].

[Yu *et al.*, 2023b] Yaodong Yu, Sam Buchanan, Druv Pai, Tianzhe Chu, Ziyang Wu, Shengbang Tong, Benjamin Haeffele, and Yi Ma. White-box transformers via sparse rate reduction. *Advances in Neural Information Processing Systems*, 36:9422–9457, 2023.

[Zhang *et al.*, 2019a] Tong Zhang, Pan Ji, Mehrtash Harandi, Richard Hartley, and Ian Reid. Scalable Deep k-Subspace Clustering. In C.V. Jawahar, Hongdong Li, Greg Mori, and Konrad Schindler, editors, *Computer Vision – ACCV 2018*, volume 11365, pages 466–481. Springer International Publishing, Cham, 2019. Series Title: Lecture Notes in Computer Science.

[Zhang *et al.*, 2019b] Tong Zhang, Pan Ji, Mehrtash Harandi, Wenbing Huang, and Hongdong Li. Neural collaborative subspace clustering. In *International Conference on Machine Learning*, pages 7384–7393. PMLR, 2019.

[Zhou *et al.*, 2018] Pan Zhou, Yunqing Hou, and Jiashi Feng. Deep adversarial subspace clustering. In *Proceedings of the IEEE conference on computer vision and pattern recognition*, pages 1596–1604, 2018.

[Zhu *et al.*, 2021] Zhihui Zhu, Tianyu Ding, Jinxin Zhou, Xiao Li, Chong You, Jeremias Sulam, and Qing Qu. A Geometric Analysis of Neural Collapse with Unconstrained Features, May 2021. arXiv:2105.02375 [cs, math, stat].

A Detailed Derivation of the Geometric Interpretation of Expansion Operators

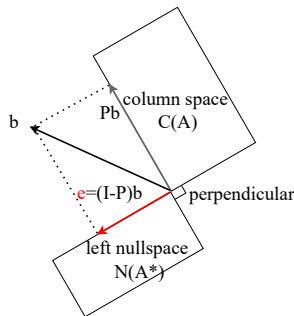


Figure 10: The Geometric Interpretation of Least Squares

Although Chan *et al.* [2022] have discussed the relationship between expansion operators and ridge regression, we further clarify their geometric interpretation by comparing the forms of the expansion operators with those of least squares and ridge regression.

For a least squares problem of $Ax = b$, the projection matrix is $P = A(A^*A)^{-1}A^*$. As show in Figure 10, its geometric meaning is to project vector b onto the column space $C(A)$. The matrix $I - P$ is also a projection matrix, which projects vector b onto the complement of column space $C(A)$,

namely the left nullspace $N(A^*)$, and the projection is the error (or residual) $e = (I - P)b$ [Strang, 2012]. For a feature z_ℓ , $E_\ell z_\ell$ can be expanded using the Woodbury identity [van Wieringen, 2023] $(I + UV)^{-1} = I - U(I + VU)^{-1}V$ as follows:

$$E_\ell z_\ell = \alpha(I - \alpha Z_\ell(I + \alpha Z_\ell^* Z_\ell)^{-1} Z_\ell^*) z_\ell. \quad (12)$$

This is exactly the *residuals* of the ridge regression problem $[\beta_\ell]_* = \arg \min_{\beta_\ell} \alpha \|z_\ell - Z_\ell \beta_\ell\|_2^2 + \|\beta_\ell\|_2^2$, which is

$$\alpha(z_\ell - Z_\ell [\beta_\ell]_*) = \alpha(I - \alpha Z_\ell(I + \alpha Z_\ell^* Z_\ell)^{-1} Z_\ell^*) z_\ell \quad (13)$$

where $[\beta_\ell]_* = \alpha(I + \alpha Z_\ell^* Z_\ell)^{-1} Z_\ell^* z_\ell$. Since the loss function of ridge regression is essentially a least squares function with an L2 norm regularization term, by analogy with the residual projection matrix $(I - P)$, we can conclude that $E_\ell z_\ell$ approximates the projection of z_ℓ 's residual onto the complement of the spanned space.

A.1 The Solution of Ridge Regression

The objective function of ridge regression problem in Eq.13 is given by:

$$[\beta_\ell]_* = \arg \min_{\beta_\ell} \alpha \|z_\ell - Z_\ell \beta_\ell\|_2^2 + \|\beta_\ell\|_2^2$$

where Z_ℓ represents the design matrix encompassing all data, z_ℓ denotes the response vector (which, in this paper, corresponds to a feature), and α is the regularization parameter. The partial derivative with respect to β_ℓ is:

$$-2\alpha Z_\ell^* (z_\ell - Z_\ell \beta_\ell) + 2\beta_\ell$$

Rearrange the gradient to zero to solve for β_ℓ :

$$-2\alpha Z_\ell^* z_\ell + 2\alpha Z_\ell^* Z_\ell \beta_\ell + 2\beta_\ell = 0$$

Rearranging terms to isolate β_ℓ on one side yields:

$$(\alpha Z_\ell^* Z_\ell + I) \beta_\ell = \alpha Z_\ell^* z_\ell$$

Solving this equation, we have:

$$[\beta_\ell]_* = \alpha(I + \alpha Z_\ell^* Z_\ell)^{-1} Z_\ell^* z_\ell$$

B The Algorithm of ESS-ReduNet

The algorithm 2 is the testing phase of ESS-ReduNet. Dynamic control is applied based on whether parameters related to Bayesian inference are detected.

C Introduction of Nearest Subspace Classifier

ReduNet acts as a feature transformation function f_θ . As demonstrated in [Yu *et al.*, 2020], each class's representations occupy low-dimensional, mutually orthogonal subspaces. Therefore, assuming that the learned features satisfy the theoretical properties, for a test sample $z_{test} = f_\theta(x_{test})$, we can classify the sample using the NSC. Formally, the predicted label is given by:

$$y = \arg \min_{j \in \{1, \dots, k\}} \|(I - U_j U_j^*) z_{test}\|_2^2 \quad (14)$$

Here, $U_j \in \mathbb{R}^{n \times r_j}$ represents the first r_j principal components of learned feature Z_j that corresponds to class j .

Algorithm 2 Testing Phase

Input: $x \in \mathbb{R}^D$, network parameters $\{\mathbf{E}_\ell\}_{\ell=1}^L$, $\{\mathbf{C}_\ell^j\}_{j=1, \ell=1}^{k, L}$, $\{w_\ell\}_{\ell=1}^L$ and $\{p_\ell^{ij}\}_{i=1, j=1, \ell=1}^{k, k, L}$, feature dimension n , λ , and a learning rate η .

Output: features z_{L+1} .

- 1: Set $z_1 = x \in \mathbb{R}^n$
 - 2: **for** $\ell = 1, \dots, L$ **do**
 - 3: **if** need Bayes **then**
 - 4: Compute corrected estimations $\{p_c^j(z_\ell)\}_{j=1}^k$.
 - 5: $z_{\ell+1} = \mathcal{P}_{\mathbb{S}^{n-1}}(z_\ell + \eta(w_\ell \mathbf{E}_\ell z_\ell - \sum_{j=1}^k \gamma_j \mathbf{C}_\ell^j z_\ell p_c^j(z_\ell)))$;
 - 6: **else if** do not need Bayes **then**
 - 7: $z_{\ell+1} = \mathcal{P}_{\mathbb{S}^{n-1}}(z_\ell + \eta(\mathbf{E}_\ell z_\ell - \sum_{j=1}^k \gamma_j \mathbf{C}_\ell^j z_\ell \hat{\pi}^j(z_\ell)))$;
 - 8: **end if**
 - 9: **end for**
-

D Detailed Experiment Results

D.1 Number of Misclassified Labels

Figures 11 to 16 illustrate the decline in misclassification rates of the estimation functions across six datasets. It is evident that in ESS-ReduNet, the decrease in misclassification rates is faster, and it achieves lower misclassification rates compared to ReduNet.

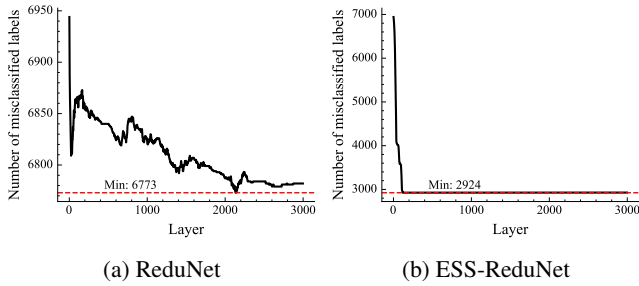


Figure 11: covtype

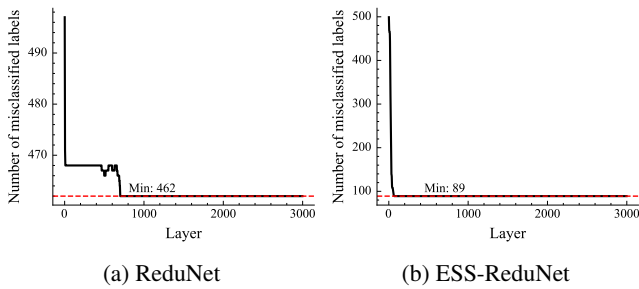


Figure 12: gas

D.2 Objective Function Curve

Figures 17 to 22 depict the curve of objective functions in six data sets, where ESS-ReduNet achieves higher values of MCR².

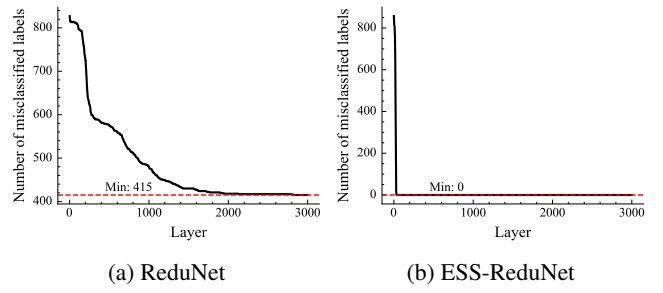


Figure 13: HAR

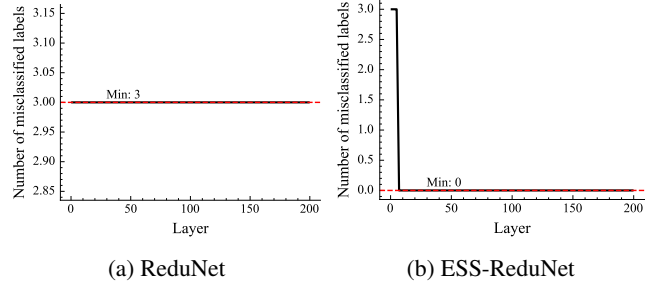


Figure 14: mfeatFactors

D.3 Rank Trend

Figures 23 to 28 show the changes in rank across six datasets. It is evident that the features transformed by ESS-ReduNet have a larger overall spanned space. Moreover, there is no occurrence of the overall spanned space collapsing, as depicted in Figure 24a.

D.4 Condition Number

Figures 29 to 34 display the changes in the condition numbers across six datasets. It is apparent that ESS-ReduNet achieves lower condition numbers more rapidly, indicating that the entire linear system stabilizes more quickly.

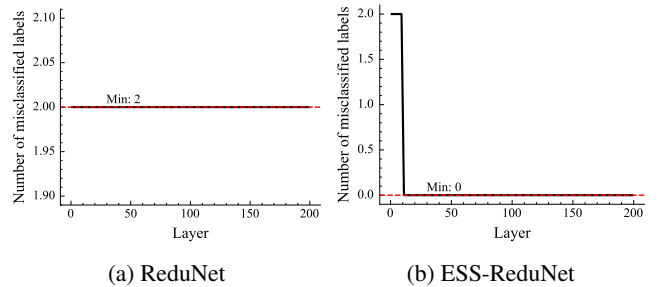
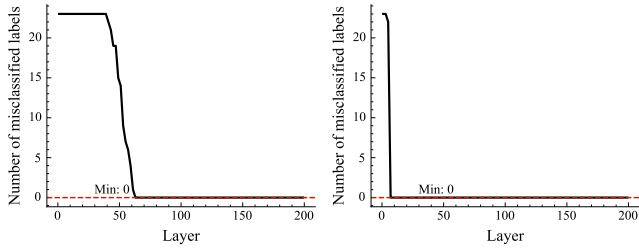


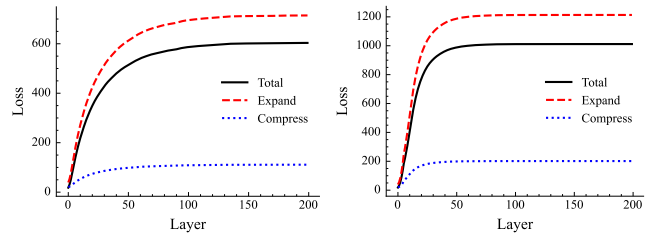
Figure 15: mfeatFourier



(a) ReduNet

(b) ESS-ReduNet

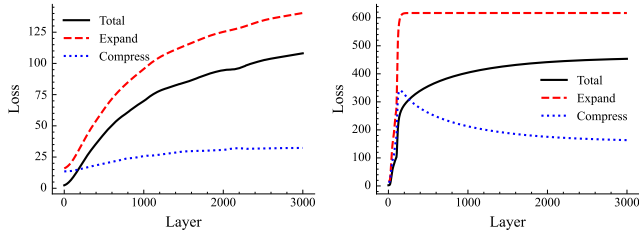
Figure 16: musk



(a) ReduNet

(b) ESS-ReduNet

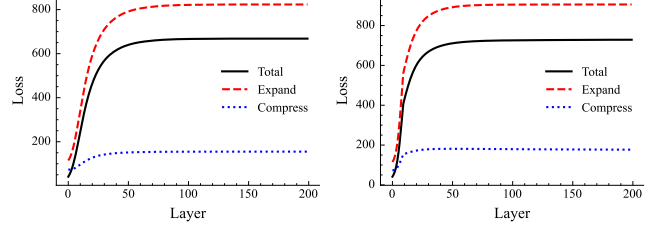
Figure 20: mfeatFactors



(a) ReduNet

(b) ESS-ReduNet

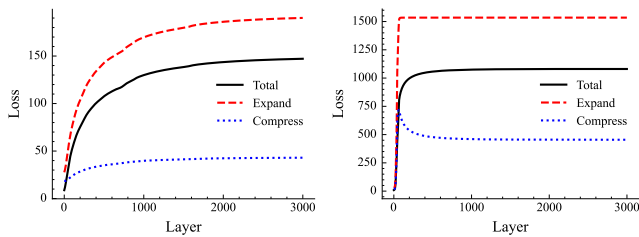
Figure 17: covtype



(a) ReduNet

(b) ESS-ReduNet

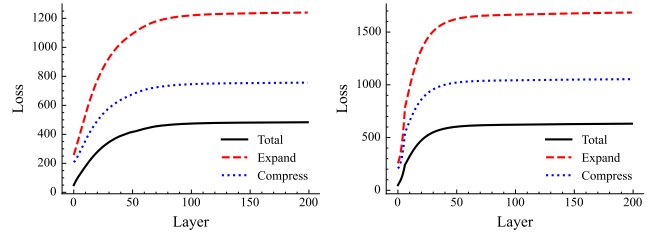
Figure 21: mfeatFourier



(a) ReduNet

(b) ESS-ReduNet

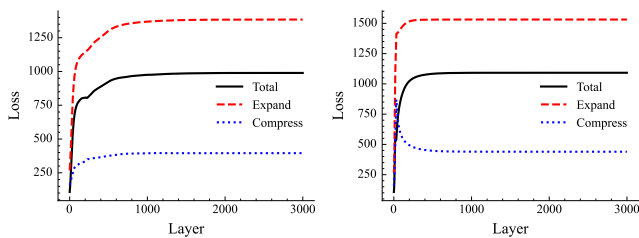
Figure 18: gas



(a) ReduNet

(b) ESS-ReduNet

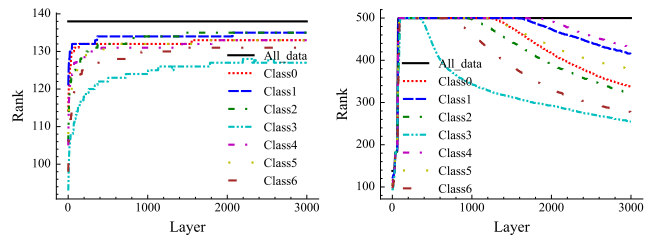
Figure 22: musk



(a) ReduNet

(b) ESS-ReduNet

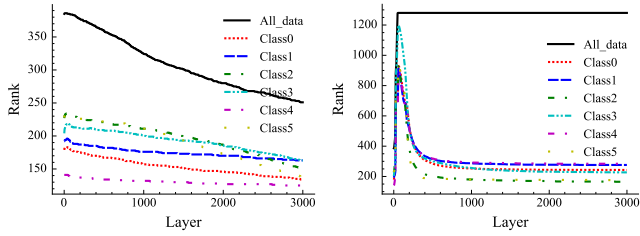
Figure 19: HARv1



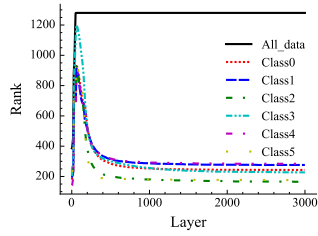
(a) ReduNet

(b) ESS-ReduNet

Figure 23: covtype

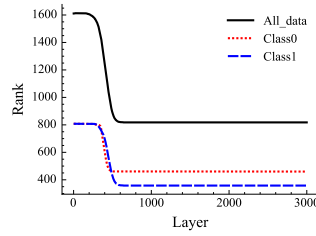


(a) ReduNet

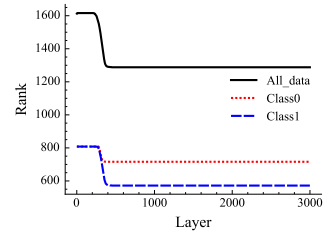


(b) ESS-ReduNet

Figure 24: gas

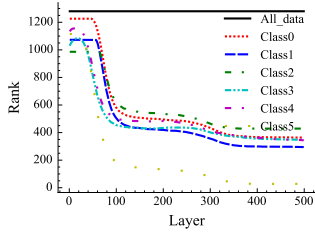


(a) ReduNet

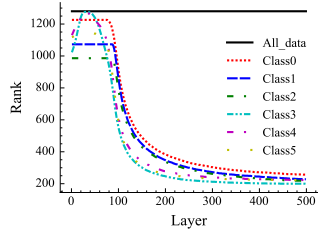


(b) ESS-ReduNet

Figure 28: musk

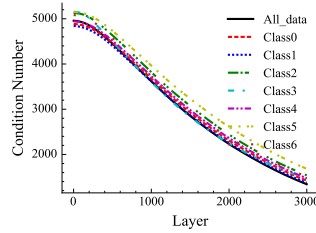


(a) ReduNet

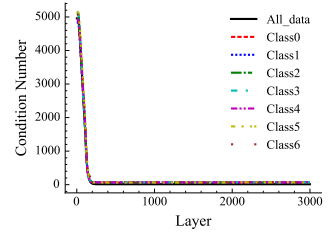


(b) ESS-ReduNet

Figure 25: HARv1

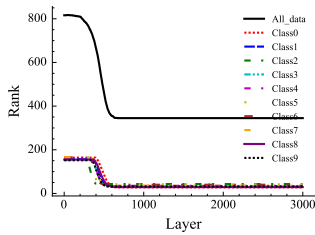


(a) ReduNet

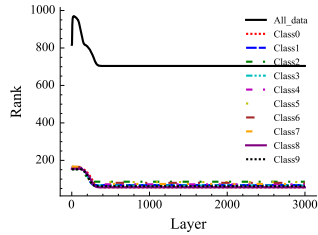


(b) ESS-ReduNet

Figure 29: covtype

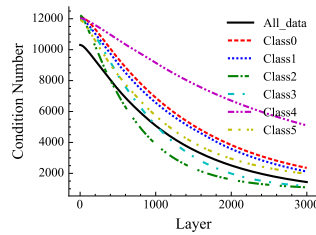


(a) ReduNet

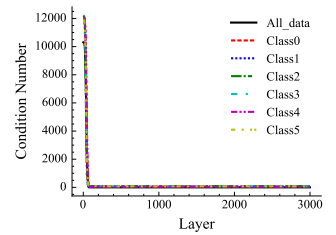


(b) ESS-ReduNet

Figure 26: mfeatFactors

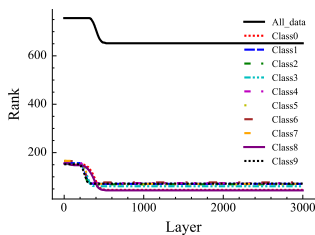


(a) ReduNet

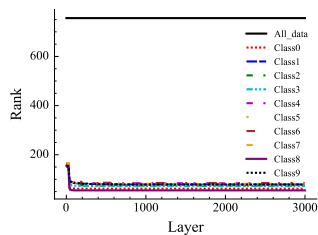


(b) ESS-ReduNet

Figure 30: gas

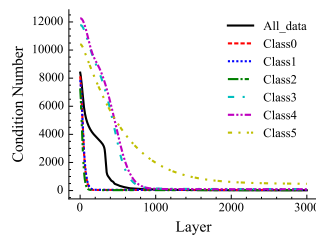


(a) ReduNet

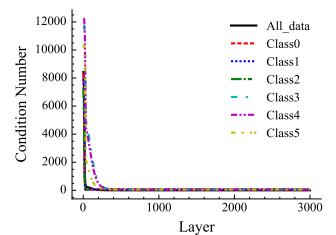


(b) ESS-ReduNet

Figure 27: mfeatFourier

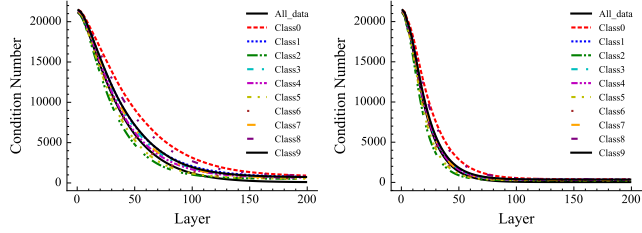


(a) ReduNet



(b) ESS-ReduNet

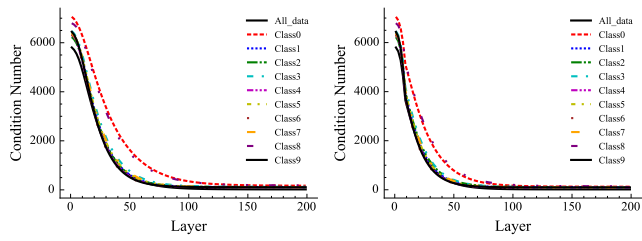
Figure 31: HARv1



(a) ReduNet

(b) ESS-ReduNet

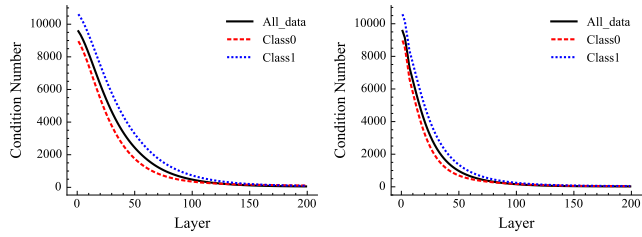
Figure 32: mfeatFactors



(a) ReduNet

(b) ESS-ReduNet

Figure 33: mfeatFourier



(a) ReduNet

(b) ESS-ReduNet

Figure 34: musk